Perturbations of whispering gallery modes by nanoparticles embedded in microcavities

K. R. Hiremath and V. N. Astratov

Department of Physics and Optical Science, Center for Optoelectronics and Optical Communications
University of North Carolina at Charlotte, NC, USA
khiremat@uncc.edu, astratov@uncc.edu

Abstract: The effects of perturbations of whispering gallery modes (WGMs) in cylindrical microcavities by embedded particles are studied by FDTD modeling. The principal effects are: i) spectral shift of the WGM-related peaks caused by the variation of the average index, ii) broadening of the WGM peaks introduced by the scattering, and iii) splitting of the WGM peaks due to formation of symmetric (SSW) and antisymmetric (ASW) standing waves. The focus of this work is on the last effect. We show that it can be maximized by placing the nanoparticle inside the cavity at a position corresponding to the antinode of the radial distribution of intensity of WGM. It is demonstrated that in this case the magnitude of splitting reaches several angstroms for 5 μm cavities with index 1.59 supporting moderately high quality ($Q \approx 10^5$) WGMs. We show that for relatively small particles with radius <70 nm and index contrasts <0.2 the magnitude of SSW/ASW splitting is linearly dependent on the size and index of the nanoparticle. This allows developing biomolecular sensors based on measuring this splitting in porous cavities. It is predicted that a similar effect of splitting can occur in semiconductor microdisks and pillars where the role of embedded dielectric nanoparticles can be played by self-assembled quantum dots.

OCIS codes: (230.5750) Resonators; (170.4520) Optical confinement and manipulation; (130.6010) Sensors, (240.0240) Optics at surfaces; (290.5850) Particles scattering

References and links

1. V. S. Ilchenko and A. B. Matsko, "Optical resonators with whispering gallery modes - Part II: Applications," IEEE J. Sel. Top. Quantum. Electron. **12**, 15-32 (2006).
2. R. W. Boyd and J. E. Heebner, "Sensitive disk resonator photonic biosensor," Appl. Opt. **40**, 5742-5747 (2001).
3. S. Arnold, M. Khoshsima, I. Teraoka, S. Holler, and F. Vollmer, "Shift of whispering-gallery modes in microspheres by protein adsorption," Opt. Lett. **28**, 272-274 (2003).
4. I. Teraoka and S. Arnold, "Theory of resonance shifts in TE and TM whispering gallery modes by nonradial perturbations for sensing applications," J. Opt. Soc. Am. B **23**, 1381-1389 (2006).
5. A. M. Armani, R. P. Kulkarni, S. E. Fraser, R. C. Flagan, K. J. Vahala, "Label-free, single-molecule detection with optical microcavities," Science **317**, 783-787 (2007).
6. D. S. Weiss, V. Sandoghdar, J. Hare, V. Lefèvre-Seguin, J.-M. Raimond, and S. Haroche, "Splitting of high-Q Mie modes induced by light backscattering in silica microspheres," Opt. Lett. **20,** 1835-1837 (1995).
7. T. Kippenberg, S. Spillane, and K. Vahala, "Modal coupling in traveling-wave resonators," Opt. Lett. **27**, 1669-1671 (2002).
8. B. E. Little, J. P. Laine, and S. T. Chu, "Surface roughness induced contradirectional coupling in ring and disk resonators," Opt. Lett., **22**, 4-6, (1997).
9. K. Srinivasan, M. Borselli, O. Painter, A. Stintz, and S. Krishna, "Cavity Q, mode volume, and lasing threshold in small diameter AlGaAs microdisks with embedded quantum dots," Opt. Express **14**, 1094-1105 (2006).
10. K. A. Fuller, "Scattering and absorption cross sections of compounded spheres. III. Spheres containing arbitrarily located spherical inhomogeneities", J. Opt. Soc. Am. A **12**, 893-904 (1995).
11. L. Pavesi, G. Panzarini, and L. C. Andreani, "All-porous silicon-coupled microcavities: Experiment versus theory," Phys. Rev. B **58**, 15794-15800 (1998).

#92009 - $15.00 USD Received 23 Jan 2008; revised 1 Apr 2008; accepted 1 Apr 2008; published 3 Apr 2008

12. V. M. Apalkov and M. E. Raikh, "Directional emission from a microdisk resonator with a linear defect," Phys. Rev. B **70**, 195317 (2004).
13. J. Wiersig and M. Hentschel, "Unidirectional light emission from high- modes in optical microcavities," Phys. Rev. A **73**, 031802 (2006).
14. E. Peter, P. Senellart, D. Martrou, A. Lemaître, J. Hours, J. M. Gérard, J. Bloch, "Exciton-photon strong-coupling regime for a single quantum dot embedded in a microcavity," Phys. Rev. Lett. **95**, 067401 (2005).
15. V. N. Astratov, S. Yang, S. Lam, B. D. Jones, D. Sanvitto, D. M. Whittaker, A. M. Fox, M. S. Skolnick, A. Tahraoui, P. W. Fry, and M. Hopkinson, "Whispering gallery resonances in semiconductor micropillars," Appl. Phys. Lett. **91**, 071115 (2007).
16. Rsoft Design Group. RSoft FullWAVE version 6.0. http://www.rsoftdesign.com
17. K. A. Fuller and D. D. Smith, "Cascaded photoenhancement from coupled nanoparticle and microcavity resonance effects", Opt. Express **15**, 3575-3580 (2007).

1. Introduction

High quality (Q) whispering gallery modes (WGMs) in microcavities can be perturbed by nanoparticles located near the surface of the cavity that can be used for sensing bacteria, proteins, DNA, and viruses [1-4]. In modestly high Q cavities ($Q \leq 10^6$) label-free biomolecular detection is typically provided due to spectral shift and broadening of the WGM resonances. The sensitivity of biomolecular sensors has been increased up to a single molecular level [5] in ultra-high $Q>10^7$ cavities due to the fact that the response of the cavity is enhanced by the heating effects caused by a nanoparticle.

One of particularly interesting effects reported for ultra-high Q microspheres [6, 7] and disks [8, 9] is connected with lifting of the degeneracy of counterpropagating (clockwise and anticlockwise) WGMs caused by surface roughness or by any perturbation near the surface. The magnitude of the observed splitting was rather small, typically in the picometer range with respect to the visible or near infrared wavelengths in these experiments.

The motivation behind this work is to investigate if this effect can be increased up to a level which would allow the development of sensor devices based on measurements of such a splitting. We focus on a situation where a nanoparticle is located inside the cavity. Such situation can be realized in microdroplets with nano-inclusions [10]. However limited index of water (1.33) or glycerol (1.47) droplets complicates observation of this effect due to reduced Q-factors of WGMs. In this work we focus on the case of cylindrical cavities with larger index (1.59). For achieving sensor functionality such structures can be realized in porous materials such as porous silicon [11]. We employed techniques of built-in sources of light to calculate spectra of WGM-related eigenstates in contrast to scattering techniques [10] used in previous studies of droplets. Emission properties of cylindrical cavities with embedded nanoparticles have been analyzed in the context of obtaining unidirectional light emission properties [12, 13], however the phenomenon of the splitting of WGM-related resonances has not been thoroughly studied in such cases.

We studied these effects for a two-dimensional (2D) model system consisting of a 5μm diameter microcylinder with index n_c=1.59 supporting WGMs with moderately high $Q \approx 1.4\times10^5$ and an embedded nanocylinder with various indices of refraction ($1<n_p<2.2$) and radii $0<R_p<120$ nm. We show that in the presence of such nanocylinder, the traveling WGMs inside microcylinder give rise to symmetric (SSW) and antisymmetric (ASW) standing waves. Due to the different overlap of SSW and ASW with the nanocylinder, they have different energies that determine the magnitude of SSW/ASW splitting. We show that by placing the nanocylinder in an optimal position inside the cavity, corresponding to the antinode of the radial intensity distribution of the WGMs, the SSW/ASW splitting reaches several angstroms in the visible regime that is easily detectable using conventional spectrometers. We study how the magnitude of the splitting depends on the location, refractive index and size of the nanocylinder. The results of these studies can be used for developing sensors based on permeable or porous materials.

It should also be noted that the results of this work have a relevance to the case of WGMs in semiconductor microdisks and micropillars with embedded quantum dots (QDs) [14, 15].

#92009 - $15.00 USD Received 23 Jan 2008; revised 1 Apr 2008; accepted 1 Apr 2008; published 3 Apr 2008

Recently such structures attracted significant interest due a possibility of strong light-matter coupling between a single QD and a high *Q* cavity mode [14] under resonant conditions. The results of our work show that besides their excitonic resonant properties, QDs can also be considered as being a nonresonant dielectric "perturbation" (due to their different index) for WGMs in a cavity, leading to the SSW/ASW splitting. Although this splitting is expected to be rather small (subangstrom), it needs to be distinguished from the Rabi splitting when interpreting the spectra of such systems.

2. Perturbation positional dependence

We start by presenting results of studies of WGM perturbations as a function of the position of a nanocylinder. The spectral response of the cavity was obtained by numerical modeling of the EM field distribution based on 2D finite difference time domain simulations using the FullWAVE^{TM} software [16]. The side excitation of WGMs was modeled by using a unidirectional source of light placed inside the cavity close to its surface, as schematically illustrated in Fig. 1(a). This source launches plane waves at a grazing angle of incidence to the cavity's sidewall that results in the building up of counterclockwise WGM traveling waves. We used a 13 fs transverse electric (TE) polarized Gaussian pulse to generate a comb of TE_l^n WGMs with radial number n=1 and various angular l numbers. To find the WGM spectra in the cavity, we performed a Fourier transform of the electric field monitored at the antinode of its radial distribution, as indicated in Fig. 1(a). The numerical convergence was checked for the calculation parameters which include spatial mesh (λ_0/30 for λ_0=540 nm) and sufficiently long time interval (400 ps). The computational domain 6x6 μm^2 was surrounded with a perfectly matching layer of width 0.5 μm.

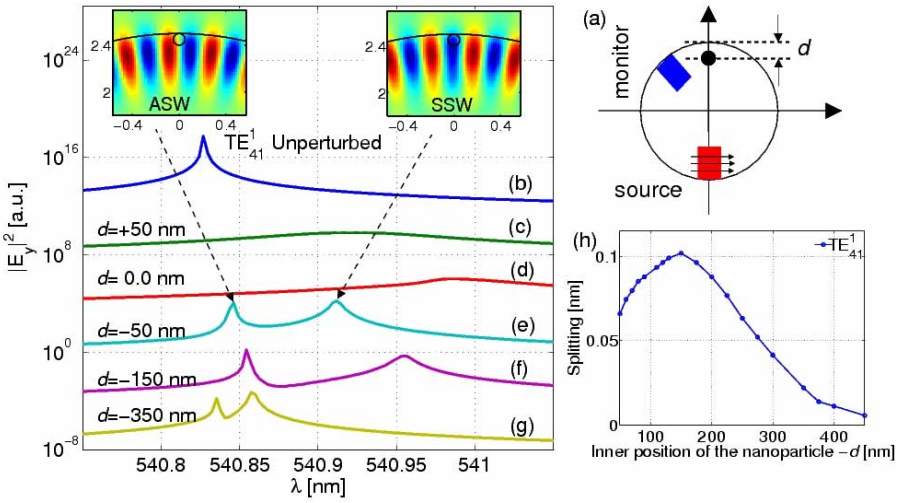

Fig. 1. (a) Sketch of the cylindrical cavity with the built-in source of light and the monitor where the field is calculated. The position of the nanocylinder is determined by distance d measured between the center of the nanocylinder and the upper edge of the cavity (d<0 means the nanocylinder is inside the cavity). (b) Spectrum of WGM resonances for an unperturbed 5μm diameter microcylinder cavity with the index n_c=1.59. Spectra (c) to (g) represent WGM peaks perturbed by a nanocylinder of radius R_p=50 nm and index n_p=1.7 located at different d. In order to separate the spectra, each successive spectrum is divided by 10^4. The insets illustrate the difference of intensity distributions for the ASW at 540.846 nm and for the SSW at 540.912 nm in terms of their overlap with the nanocylinder. (h) The dependence of SSW/ASW splitting on the position of nanocylinder represented by d.

For comparison purposes we presented in Fig. 1(b) a WGM spectrum of an unperturbed cavity (without a nanocylinder). This spectrum illustrates a TE_{41}^1 WGM peak at 540.83 nm with $Q\approx1.4\times10^5$. The spectra presented in Figs. 1(c-g) illustrate the effects of WGM perturbation by the nanocylinder located at various depths d.

#92009 - $15.00 USD Received 23 Jan 2008; revised 1 Apr 2008; accepted 1 Apr 2008; published 3 Apr 2008

As illustrated in Fig. 1(c), when the nanocylinder is outside the microcylinder (d= 50 nm), the main effect is a dramatic broadening of the WGM resonance (Q≈3100) caused by the scattering losses introduced by the nanocylinder. The shift of the peak by 0.093 nm is determined by the increased effective index experienced by the WGM in microcylinder. Similar effects are obtained for the nanocylinder located at the surface of the cavity (d=0), as illustrated in Fig. 1(d). In this case, an increased long wavelength shift of the resonance is due to the larger overlap of WGM EM field with the high index nanocylinder (n_p=1.7). Generally, our results show that the broadening effects can be significant in such cases. It should be noted however that for smaller perturbations ($\Delta n = n_p - n_c < 0.1$, $R_p << 50$ nm) the resonance was found to be not spoiled to a significant degree in qualitative agreement with the analytical theory [4] and with the results of modeling for droplets [10] and microspheres [17].

As represented in Fig. 1(e) when the nanocylinder is completely embedded in the cavity touching its surface from inside (d=−50 nm), the perturbation manifests itself by the appearance of a double peak structure. An increased scattering of the WGM by the nanocylinder in a backward direction leads in this case to the formation of clockwise traveling WGMs. Both counterpropagating waves are phase matched and their interference leads to the formation of an antisymmetric standing wave (ASW) peak at 540.846 nm and a symmetric standing wave (SSW) peak at 540.912 nm.

The splitting between ASW and SSW peaks can be qualitatively explained by the different overlap of these waves with the high index material represented by the nanocylinder. This interpretation is supported by calculations of the WGM intensity distributions for two peaks at 540.846 nm and 540.912 nm, as illustrated in insets at the top of Fig. 1. In these calculations, we propagated longer pulses with the bandwidths comparable to the widths of these spectral peaks, and with the center wavelength resonant with the peak positions. By analyzing the time evolution of these intensity maps, we verified that both resonances are indeed standing waves as opposed to an uncoupled traveling TE_{41}^{1} WGM at 540.83 nm in Fig. 1(b). For ASW at 540.846 nm the overlap of intensity pattern with the nanocylinder is minimized (left inset), since the intensity has a zero at the center of nanocylinder. This explains not only the shorter wavelength of ASW, but also the fact that this wave does not effectively interact with the nanocylinder. This results in nearly the same Q-factor (≈ 10^5) of this peak as in the reference structure illustrated in Fig. 1(b). In contrast, the SSW at 540.912 nm has a maximum at the center of nanoparticle (right inset) that explains both a smaller Q-factor (≈ 10^4) observed for this peak and its location at a longer wavelength.

If the nanoparticle is placed deeper (d=−150 nm) inside the cavity, the resulting perturbation of the WGM increases which is seen due to increased splitting in Fig. 1(f). But when the particle moves in the cavity deeper than the antinode of the radial intensity distribution of TE_{41}^{1}, the WGM perturbation is reduced, as illustrated by smaller SSW/ASW splitting at d= −350 nm in Fig. 1(g). The plot in Fig 1(h) shows this dependence of the splitting on the radial position of the nanoparticle. It is seen that the maximal SSW/ASW splitting is achieved for nanocylinder located at the radial antinode of WGMs at d=−150 nm.

3. Index contrast dependence

The dependence of the positions of SSW and ASW peaks originating from TE_{41}^{1} peak on the refractive index contrast of perturbation, $\Delta n = n_p - n_c$, is shown in Fig. 2(a). In these calculations we fix the position of the nanocylinder at $d = -R_p = -50$ nm corresponding to the situation illustrated in Fig. 1(e). Generally, the positions of the peaks are determined by the average index experienced by the corresponding waves. The ASW peak is found to be shifting only slightly with Δn, as illustrated by the red dashed line in Fig. 2(a). It is interesting to note that this peak was also found to have almost the same $Q \approx 10^5$ in a very broad range of index contrasts, $-0.6 < \Delta n < 0.7$, as illustrated in Fig. 2(b). As it was already mentioned in the previous paragraph, this behavior is due to the small overlap of ASW with the nanocylinder. In contrast, SSW has maximal overlap with the nanocylinder that results in very strong shift of this peak with Δn, as illustrated in Fig. 2(a) by the blue dashed line. Strong scattering of SSW

#92009 - $15.00 USD Received 23 Jan 2008; revised 1 Apr 2008; accepted 1 Apr 2008; published 3 Apr 2008

by the nanocylinder also explains pronounced decay of Q-factor of this wave with Δn, as illustrated in Fig. 2(b).

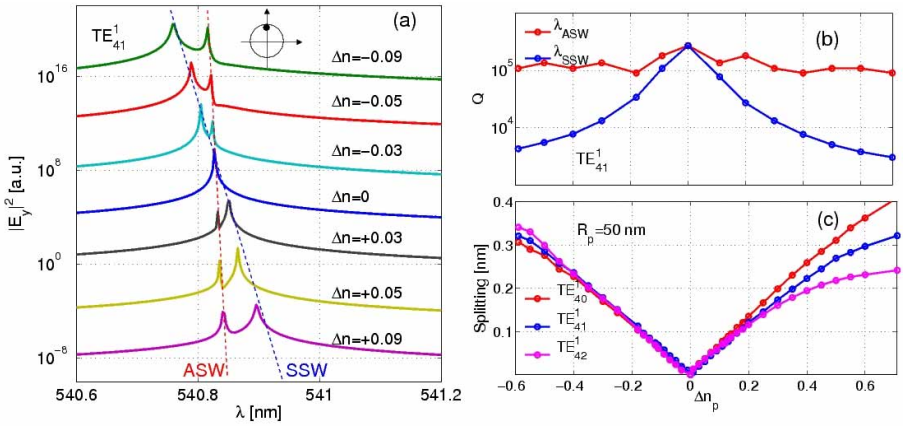

Fig. 2. (a) Dependence of WGM spectra on the index contrast $\Delta n = n_p - n_c$ of the perturbation. The red dashed line and the blue dashed line show behavior of ASW peak and SSW peak respectively. The perturbation setting is as shown in the inset. The size of the cavity and the nanocylinder, and the spectrum scaling is the same as that for Fig. 1. Dependence of (b) quality factors and (c) splitting of SSW and ASW peaks on the index contrast Δn of the perturbation.

Fig. 2(c) shows the dependence of the splitting ($|\lambda_{SSW} - \lambda_{ASW}|$) between SSW and ASW peaks on the perturbation index contrast. The results are presented for three SSW/ASW pairs of peaks originating from unperturbed WGM peaks TE_{40}^{1}, TE_{41}^{1}, and TE_{42}^{1}. It is found that the splitting behaves linearly in the limit of small contrasts. For $|\Delta n|>0.2$ however the splitting displays a marked nonlinear behavior that indicates that such a particle can no longer be considered as a small perturbation. Thus, the results presented in Fig. 2(c) show that SSW/ASW splitting of the order of several angstroms can be caused by the embedded particles with R_p=50 nm and the amount of splitting is proportional to the index contrast introduced by the nanoparticle.

4. Perturbation size dependence

In the previous analysis the particle was assumed to be small compared to the wavelength in the medium (R_p=50 nm << λ_0/n~340 nm). It is interesting to consider the case of larger nanoparticles where the behavior of ASW resonances should be very different due to the fact that the field can become quite significant at the edges of the particle despite that it has a null at the center of the particle.

In order to model the behavior of ASW for larger particles we used a similar setting with the nanocylinder with index n_p=1.64 placed at $d=-R_p$ that corresponds to the case of the nanocylinder touching the surface of microcylinder from inside. The radius of the nanocylinder was varied from $0<R_p<300$ nm. The dependence of both peak (SSW and ASW) positions on R_p is presented in Fig. 3(a) for a WGM originating from TE_{41}^{1} resonances. It can be seen that in the limit of small sizes ($R_p \leq 50$ nm), as expected, the red curve in Fig. 3(a) representing the ASW peak shows nearly the same wavelength (=540.83 nm = resonance wavelength of the unperturbed TE_{41}^{1}), however for larger particles it shows an increasing long wavelength shift. It is interesting to note that for particles with $R_p>80$ nm the slope of the red curve exceeds that of the blue curve (representing SSW peak) which leads to the crossing of these curves around R_p=105 nm.

In Fig. 3(b) we plotted the dependence of splitting between SSW and ASW pairs of peaks as a function of R_p calculated for two different WGM resonances. All dependences demonstrate pronounced minima around R_p=105 nm, where both SSW and ASW EM field have the same degree of overlap with the embedded particle. The behavior of the curves in

#92009 - $15.00 USD Received 23 Jan 2008; revised 1 Apr 2008; accepted 1 Apr 2008; published 3 Apr 2008

Fig. 3(a) indicates a crossing rather than anticrossing trend around R_p=105 nm, since the on-resonance SSW/ASW splitting is found to be smaller than the linewidths of the individual peaks. Because of the difficulty of determining such small splittings, they are not shown in Fig. 3(b) below the horizontal cut-off line at 0.01 nm.

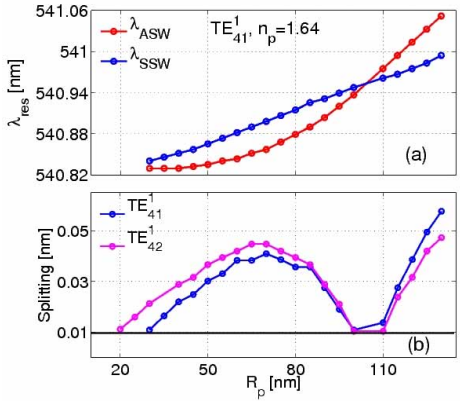

Figure 3. Dependencies of (a) SSW and ASW peak positions and (b) SSW/ASW splitting on the radius (R_p) of the nanocylinder (n_p=1.64) embedded at d= $-R_p$ deep inside 5 μm microcylinder (n_c=1.59). The rest of the simulation setting is as for Fig. 2.

5. Conclusions

The optical phenomena studied in this paper are determined in a fundamental way by the effect of the formation of standing WGMs in a cylindrical cavity caused by embedded nanoparticles. A similar effect has been known [6-9] for the surface perturbations. We found that by placing the nanoparticle at the antinode of the radial distribution of intensity of WGMs, it is possible to achieve SSW/ASW splittings of the order of several angstroms for cavities with moderately high quality ($Q\approx10^5$) WGMs. Such cavities can be realized in permeable or porous materials such as porous silicon, and can be characterized by using conventional spectroscopic tools. We showed that in the limit of relatively small particles (R_p<50 nm) with limited index contrasts (Δn<0.2) the splitting between SSW and ASW peak is linearly dependent on the size and index of the nanoparticle. This suggests the possiblity of developing biomolecular sensors based on the measurement of this splitting. If bacteria, proteins, DNA, and viruses are trapped at an optimal depth inside the cavity, they should produce a certain SSW/ASW splitting which can be used to identify these nano-objects. The values of the splitting determined in this work on the basis of 2D modeling can be used as a rough estimate of the effects which are expected to be observed in such 3D cases.

On the basis of the simple 2D model used in this work, it is possible to suggest that similar SSW/ASW splitting phenomena can take place in completely different material systems, e.g. as semiconductor microdisks [14] and pillars [15] with quantum dots. Self-organized QDs can play the part of embedded dielectric particles causing perturbations of WGMs in semiconductor cavities. This should result in a subangstrom SSW/ASW splitting which should be clearly distinguished from the normal mode splitting phenomena arising from strong coupling with the excitonic oscillator. Thus the results of this work can be useful for interpreting spectroscopic studies of high Q semiconductor cavities and photonic molecules with embedded quantum dots.

Acknowledgments

The authors are thankful to S. Arnold for discussions which initiated this work. We also thank M.A. Fiddy for stimulating discussions. These works was supported by ARO grant W911NF-05-1-0529 and by NSF grant CCF-0513179 as well as, in part, by funds provided by the University of North Carolina at Charlotte. K. R. Hiremath also acknowledges funding by DARPA Grant No. W911NF-05-2-0053.

#92009 - $15.00 USD Received 23 Jan 2008; revised 1 Apr 2008; accepted 1 Apr 2008; published 3 Apr 2008